Chapter 2
Conduction Heating of Solid Surfaces

Abstract Laser conduction heating involves with a solid phase heating for a stationary or moving sources. In order to accommodate the absorption of irradiated laser energy, a volumetric source consideration should be incorporated. Since the analytical solution for such heating situation is possible, a closed form solution for the temperature field is provided firstly. In order to assess the influence of duty cycle on the temperature field, a numerical model is introduced. To study the thermal effects, two-dimensional axisymmetric solid is considered for a stationary source and three-dimensional heating situation is incorporated for a moving source in the model studies. The laser heating is involved with the assisting gas processing; therefore, the convection effect of the assisting gas is incorporated in the analysis. Since the heating duration is longer than the thermalization time of the substrate material for most of the surface treatment processes, the Fourier heating law is incorporated in the analysis. In this chapter, Laser conduction heating of solid surfaces is introduced and analytical approaches for temperature field in the irradiated region is presented for the appropriate boundary and heating conditions.

2.1 Introduction

Laser conduction heating involves with a solid phase heating for a stationary or moving sources. In order to accommodate the absorption of irradiated laser energy, a volumetric source consideration should be incorporated. Since the analytical solution for such heating situation is possible, a closed form solution for the temperature field is provided firstly. In order to assess the influence of duty cycle on the temperature field, a numerical model is introduced. To study the thermal effects, two-dimensional axisymmetric solid is considered for a stationary source and three-dimensional heating situation is incorporated for a moving source in the model studies. The laser heating is involved with the assisting gas processing; therefore, the convection effect of the assisting gas is incorporated in the analysis.

B. S. Yilbas and S. Z. Shuja, *Laser Surface Processing and Model Studies*, Materials Forming, Machining and Tribology, DOI: 10.1007/978-3-642-36629-1_2,

Since the heating duration is longer than the thermalization time of the substrate material for most of the surface treatment processes, the Fourier heating law is incorporated in the analysis.

2.2 Analytical Treatment of Laser Pulse Heating

Closed form solution of the pulse laser heating of the solid surfaces enables to identify the affecting parameters through analytical expressions developed between the temperature field and the parameters. The closed form solution for laser repetitive pulse heating, therefore, becomes fruitful when examining the possibility of the steady heating at the surface by the laser repetitive pulses. Laser pulse heating of the solid substrates requires formulation of laser pulses due to the fact that laser intensity varies with time. This results in different heating situations due to temporal laser pulse behavior. In this case, two heating situations can be considered to account for the temporal behavior of the laser pulse intensity. The first case is involved with a single exponential pulse heating and the other case is the heating due to the multi-pulses (repetitive pulses). The closed form solutions for each cases is presented according to the below sub-headings.

2.2.1 Exponential Pulse Heating

The analytical formulation of laser pulse heating of solid substrate with a convective boundary condition at the surface is considered in the light of the previous study [1]. The time exponentially varying pulse intensity is incorporated in the analysis provided that two different pulse types are taken into account. In the first pulse type (half pulse), the intensity decays exponentially with time $(I_1 \exp(-\beta'\tau))$ while the intensity distribution resembling a typical actual laser pulse $I_1[\exp(-\beta'\tau) - \exp(-\gamma'\tau)]$ is considered in the second pulse type (full pulse). The closed-form solution obtained from the present study is compared with the previous formulations for the appropriate pulse and boundary conditions. The heating analysis is carried out for nanosecond laser pulses, which is longer than the thermalization time of the metal substrates; therefore, the Fourier theory of heating is used when modeling the heating process [2]. The heat transfer equation for a laser heating pulse can be written as:

$$\frac{\partial^2 T}{\partial x^2} + \frac{I_1 \delta}{k}(e^{-\beta t} - e^{-\gamma t})e^{\delta x} = \frac{1}{\alpha}\frac{\partial T}{\partial t} \tag{2.1}$$

where I_1 is the power intensity, δ is the absorption depth, β and γ are the pulse parameters, and α is the thermal diffusivity.

The output pulse from a laser can be formulated through subtracting two exponential functions. Hence, the power intensity distribution of time exponentially varying pulse can be written as:

$$I = I_1\left(e^{-\beta t} - e^{-\gamma t}\right) \tag{2.2}$$

where $I_1 = \left(1 - r_f\right)I_0$ and r_f is the reflection coefficient and I_o is the peak power intensity, and parameters β and γ can be chosen to give the appropriate rise time for the pulse. Since the governing equation of heat transfer is linear (Eq. 2.1) the closed form solution can be obtained for a half pulse first, then, the complete solution can be achieved by subtraction of the solutions for the individual parts of the time exponential pulse (half pulse). It should be noted that for the solution of full pulse, the ambient temperature is considered as zero $(T_0 = 0)$. This is necessary since the full pulse solution satisfies the convective boundary condition when $T_0 = 0$. The heat transfer equation for the half pulse becomes:

$$\frac{\partial^2 T}{\partial x^2} + \frac{I_1\delta}{k}e^{-(\beta t + \delta x)} = \frac{1}{\alpha}\frac{\partial T}{\partial t} \tag{2.3}$$

The absorption depth of the substrate material is considerable smaller than the thickness of the substrate material. This allows one to consider the semi-infinite solid body, initially at uniform temperature, with convective boundary condition at the surface. It should be noted that convective boundary condition at the surface resembles the assisting gas jet effect at the surface of the solid substrate during the heating process. Therefore, the initial and boundary conditions are:

at time t = 0	$T(x,0) = 0$
at the surface $x = 0$	$\left[\frac{\partial T}{\partial x}\right]_{x=0} = \frac{h}{k}(T(0,t) - T_o)$
and at $x = \infty$	$T(t,\infty) = 0$

The solution of Eq. 2.3 can be obtained possibly through Laplace transformation method, i.e., with respect to t, the Laplace transformation of Eq. 2.3 yields:

$$\frac{\partial^2 \overline{T}}{\partial x^2} + \frac{I_1\delta}{k}e^{-\delta x}\frac{1}{p+\beta} = \frac{1}{\alpha}\left[p\overline{T} - T(x,0)\right] \tag{2.4}$$

where $\overline{T} = T(x,p)$ and $T(x,0) = 0$ due to the initial condition. Using the initial condition, Eq. 2.4 yields:

$$\frac{\partial^2 \overline{T}}{\partial x^2} - \frac{p\overline{T}}{\alpha} = -\frac{I_1\delta}{k}e^{-\delta x}\frac{1}{p+\beta} \tag{2.5}$$

Let consider $\lambda^2 = \frac{p}{\alpha}$ and $H_o = -\frac{I_1\delta}{k}\frac{1}{(p+\beta)}$, then Eq. 2.5 becomes:

$$\frac{\partial^2 \overline{T}}{\partial x^2} - \lambda^2 \overline{T} = H_o e^{-\delta x} \tag{2.6}$$

Equation 2.6 has homogeneous $\left(\overline{T}_h\right)$ and particular solutions $\left(\overline{T}_p\right)$, i.e.:

$$\overline{T} = \overline{T}_h + \overline{T}_p \tag{2.7}$$

The homogeneous solution is:

$$\overline{T}_h = C_1 e^{\lambda x} + C_2 e^{-\lambda x} \tag{2.8}$$

where C_1 and C_2 are the constants to be determined from the boundary conditions. Similarly the particular solution is:

$$\overline{T}_p = A_o e^{-\delta x} \tag{2.9}$$

where A_o is the constant.

Equation 2.7 yields the solution:

$$A_o \delta^2 e^{-\delta x} - \lambda^2 A_o e^{-\delta x} = H_o e^{-\delta x} \tag{2.10}$$

or

$$A_o = \frac{H_o}{(\delta^2 - \lambda^2)} \tag{2.11}$$

After the rearrangement, the particular solution $\left(\overline{T}_p\right)$ results:

$$\overline{T}_p = \frac{H_o}{(\delta^2 - \lambda^2)} e^{-\delta x} \tag{2.12}$$

Therefore, the solution of Eq. 2.4 in the Laplace domain becomes:

$$\overline{T} = \overline{T}(x, p) = C_1 e^{\lambda x} + C_2 e^{-\lambda x} + \frac{H_o}{(\delta^2 - \lambda^2)} e^{-\delta x} \tag{2.13}$$

The coefficients in Eq. 2.13 can be obtained from the boundary conditions. Consider $\lambda = \sqrt{\frac{p}{\alpha}} > 0$ and from the boundary condition $T(\infty, t) = 0$ result in $C_1 = 0$. Moreover, let $\overline{H}_0 = \frac{H_0}{(\delta^2 - \lambda^2)}$, Eq. 2.13 becomes:

$$\overline{T} = C_2 e^{-\lambda x} + \overline{H}_o e^{-\delta x} \tag{2.14}$$

In order to determine C_2, the boundary condition at the surface can be incorporated, i.e.:

$$\left[\frac{\partial \overline{T}}{\partial x}\right]_{x=0} = \frac{h}{k}\left[\overline{T}(0, p) - \frac{T_o}{p}\right] \tag{2.15}$$

where T_0, which is an ambient temperature (same as the initial temperature), can be specified. Introducing Eq. 2.14 into Eq. 2.15 and knowing that $\overline{T}(0,p) = C_2 + \overline{H}_o$, it yields:

$$-\lambda C_2 - \delta \overline{H}_o = \frac{h}{k}\left[C_2 + \overline{H}_o - \frac{T_o}{p}\right] \tag{2.16}$$

Hence, C_2 becomes:

$$C_2 = -\frac{\overline{H}_o(h + k\delta)}{(h + k\lambda)} + \frac{T_o h}{p(h + k\lambda)} \tag{2.17}$$

Substituting C_2 and the values of H_o, $\overline{H}_o$ and λ into Eq. 2.14, it becomes:

$$\overline{T}(x,p) = \frac{I_1\delta(h + k\delta)e^{-\sqrt{\frac{p}{\alpha}}x}}{k(p+\beta)\left(\delta^2 - \frac{p}{\alpha}\right)\left(h + \frac{k\sqrt{p}}{\sqrt{\alpha}}\right)} + \frac{T_o h e^{-\sqrt{\frac{p}{\alpha}}x}}{p\left(h + \frac{k\sqrt{p}}{\sqrt{\alpha}}\right)} - \frac{I_1\delta}{k(p+\beta)\left(\delta^2 - \frac{p}{\alpha}\right)}e^{-\delta x} \tag{2.18}$$

The mathematical arrangements of inversion of Eq. 2.18 is given in the previous study [1]. Therefore, the Laplace inversion of Eq. 2.18 becomes:

$$\begin{aligned} T(x,\,t) = a_{10}\Bigg\{ & \sqrt{\beta}ie^{-\beta t}\left[-l_1 e^{\sqrt{\frac{\beta}{\alpha}}ix}\mathrm{erfc}\left(\sqrt{\beta t}i + \tfrac{x}{2\sqrt{\alpha t}}\right) + l_2 e^{-\sqrt{\frac{\beta}{\alpha}}ix}\mathrm{erfc}\left(-\sqrt{\beta t}i + \tfrac{x}{2\sqrt{\alpha t}}\right)\right] \\ & +\delta\sqrt{\alpha}e^{\alpha\delta^2 t}\left[l_3 e^{-\delta x}\mathrm{erfc}\left(-\delta\sqrt{\alpha t} + \tfrac{x}{2\sqrt{\alpha t}}\right) - l_4 e^{\delta x}\mathrm{erfc}\left(\delta\sqrt{\alpha t} + \tfrac{x}{2\sqrt{\alpha t}}\right)\right] \\ & -w_1 l_5 e^{w_1\frac{x}{\sqrt{\alpha}}}e^{w_1^2 t}\mathrm{erfc}\left(w_1\sqrt{t} + \tfrac{x}{2\sqrt{\alpha t}}\right) \Bigg\} \\ & + \frac{a_{20}}{(\beta + \alpha\delta^2)}(e^{\alpha\delta^2 t} - e^{-\beta t})e^{-\delta x} \\ & + \frac{a_{30}}{w_1}\left[-e^{w_1\frac{x}{\sqrt{\alpha}}}e^{w_1^2 t}\mathrm{erfc}\left(w_1\sqrt{t} + \frac{x}{2\sqrt{\alpha t}}\right) + \mathrm{erfc}\left(\frac{x}{2\sqrt{\alpha t}}\right)\right] \end{aligned} \tag{2.19}$$

where

$$\begin{aligned} l_1 &= \frac{1}{2\sqrt{\beta}i(\beta + \alpha\delta^2)(-\sqrt{\beta}i + w_1)} : l_2 = -\frac{1}{2\sqrt{\beta}i(\beta + \alpha\delta^2)(\sqrt{\beta}i + w_1)} \\ l_3 &= \frac{1}{2\sqrt{\alpha}\delta(\beta + \alpha\delta^2)(\delta\sqrt{\alpha} + w_1)} : l_4 = -\frac{1}{2\sqrt{\alpha}\delta(\beta + \alpha\delta^2)(-\delta\sqrt{\alpha} + w_1)} \\ l_5 &= \frac{1}{(w_1^2 + \beta)(w_1^2 - \alpha\delta^2)} \end{aligned} \tag{2.20}$$

and

$$a_{10} = -\frac{I_1\alpha\sqrt{\alpha}\delta(h + k\delta)}{k^2} : a_{20} = \frac{I_1\alpha\delta}{k} : a_{30} = \frac{h\sqrt{\alpha}}{k}T_o : w_1 = \frac{h\sqrt{\alpha}}{k} \tag{2.21}$$

After inserting l_1, l_2, l_3, l_4, l_5, a_{10}, a_{20}, a_{30}, and w_1, Eq. 2.19 becomes:

$$T(x,t) = \frac{I_1\alpha\sqrt{\alpha}\delta(h+k\delta)}{k^2}\left\{\begin{array}{c} -\frac{e^{-\delta x}e^{\alpha\delta^2 t}\mathrm{erf}\,c\left(\frac{x}{2\sqrt{\alpha t}}-\delta\sqrt{\alpha t}\right)}{2(\beta+\alpha\delta^2)\left(\frac{h\sqrt{\alpha}}{k}+\delta\sqrt{\alpha}\right)} - \frac{e^{\delta x}e^{\alpha\delta^2 t}\mathrm{erf}\,c\left(\frac{x}{2\sqrt{\alpha t}}+\delta\sqrt{\alpha t}\right)}{2(\beta+\alpha\delta^2)\left(\frac{h\sqrt{\alpha}}{k}-\delta\sqrt{\alpha}\right)} \\ +\frac{e^{-\beta t}e^{\sqrt{\frac{\beta}{\alpha}}xi}\mathrm{erf}\,c\left(\frac{x}{2\sqrt{\alpha t}}+\sqrt{\beta t}i\right)}{2(\beta+\alpha\delta^2)\left(\frac{h\sqrt{\alpha}}{k}-\sqrt{\beta}i\right)} + \frac{e^{-\beta t}e^{-\sqrt{\frac{\beta}{\alpha}}xi}\mathrm{erf}\,c\left(\frac{x}{2\sqrt{\alpha t}}-\sqrt{\beta t}i\right)}{2(\beta+\alpha\delta^2)\left(\frac{h\sqrt{\alpha}}{k}+\sqrt{\beta}i\right)} \\ +\frac{h\sqrt{\alpha}}{k}\frac{e^{\frac{hx}{k}}e^{\frac{h^2}{k^2}\alpha t}\mathrm{erf}\,c\left(\frac{x}{2\sqrt{\alpha t}}+\frac{h}{k}\sqrt{\alpha t}\right)}{k\left(\frac{h^2\alpha}{k^2}+\beta\right)\left(\frac{h^2\alpha}{k^2}-\alpha\delta^2\right)} - \frac{k\sqrt{\alpha}e^{-\delta x}(e^{-\alpha\delta^2 t}-e^{-\beta x})}{(\beta+\alpha\delta^2)(h+k\delta)} \end{array}\right\}$$
$$+ T_o\left[\mathrm{erf}\,c\left(\frac{x}{2\sqrt{\alpha t}}\right) - e^{\frac{hx}{k}}e^{\frac{h^2}{k^2}\alpha t}\mathrm{erf}\,c\left(\frac{x}{2\sqrt{\alpha t}}+\frac{h}{k}\sqrt{\alpha t}\right)\right] \tag{2.22}$$

The surface temperature can be obtained when setting x equals to zero ($x = 0$) in Eq. 2.22. The mathematical arrangements are given in the previous study [1]. Therefore, the resulting surface temperature becomes:

$$T(0.t) = \frac{I_1\alpha\delta}{(\beta+\alpha\delta^2)(\beta k^2+\alpha h^2)}\left[(\alpha\delta h-\beta k)e^{-\beta t} + 2\sqrt{\frac{\alpha\beta}{\pi}}(h+\delta k)F(\sqrt{\beta t})\right]$$
$$+\frac{I_1\alpha\delta^2}{(\delta k-h)(\beta+\alpha\delta^2)}e^{\alpha\delta^2 t}\mathrm{erf}\,c(\delta\sqrt{\alpha t})$$
$$-\left(T_o - \frac{I_1\alpha\delta hk}{(\beta k^2+\alpha h^2)(h-\delta k)}\right)e^{\frac{h^2\alpha t}{k^2}}\mathrm{erf}\,c\left(\frac{h}{k}\sqrt{\alpha t}\right) + T_o \tag{2.23}$$

In order to reduce Eq. 2.23 in dimensionless form, the following non-dimensional parameters are introduced:

$$\beta' = \frac{\beta}{\alpha\delta^2} : h' = \frac{h}{\delta k} : \tau = \alpha\delta^2 t \tag{2.24}$$

After mathematical arrangement and incorporating Eqs. 2.24, 2.23 yields:

$$T(0,\tau) = \frac{I_1}{\delta k}\frac{1}{(1+\beta')(\beta'+h'^2)}\left[(h'-\beta')e^{-\beta'\tau} + \frac{2}{\sqrt{\pi}}\sqrt{\beta'}(1+h')F\left(\sqrt{\beta'\tau}\right)\right]$$
$$+\frac{I_1}{\delta k}\frac{1}{(1-h')(1+\beta')}e^{\tau}\mathrm{erf}\,c\left(\sqrt{\tau}\right)$$
$$-\left[T_o - \frac{I_1}{\delta k}\left(\frac{h'}{(\beta'+h'^2)(h'-1)}\right)\right]e^{h'^2\tau}\mathrm{erf}\,c\left(h'\sqrt{\tau}\right) + T_o \tag{2.25}$$

where $F(\chi)$ is Dawson's integral, which is:

$$F(\chi) = e^{-\chi^2} \int_0^{\chi} e^{\xi^2} d\xi \tag{2.26}$$

The complete solution for the heating pulse (full pulse) can be obtained through incorporating the principle of superposition; in which case, after subtracting the solutions of the temperature profile for two exponential terms $\left(e^{-\beta t}\right.$ and $\left.e^{-\gamma t}\right)$ as used in the full pulse profile, the complete solution for the full pulse becomes:

$$\begin{aligned} T(0,\tau) = {} & \frac{I_1}{\delta k} \frac{1}{(1+\beta')(\beta'+h'^2)} \left[(h'-\beta') e^{-\beta'\tau} + \frac{2}{\sqrt{\pi}} \sqrt{\beta'}(1+h') F\left(\sqrt{\beta'\tau}\right) \right] \\ & + \frac{I_1}{\delta k} \frac{1}{(1-h')(1+\beta')} e^{\tau} \operatorname{erf} c(\sqrt{\tau}) \\ & + \frac{I_1}{\delta k} \frac{h'}{(\beta'+h'^2)(1-h')} e^{h'^2\tau} \operatorname{erf} c(h'\sqrt{\tau}) \\ & \frac{I_1}{\delta k} \frac{1}{(1+\gamma')(\gamma'+h'^2)} \left[(h'-\gamma') e^{-\gamma'\tau} + \frac{2}{\sqrt{\pi}} \sqrt{\gamma'}(1+h') F(\gamma'\tau) \right] \\ & + \frac{I_1}{\delta k} \frac{1}{(1-h')(1+\gamma')} e^{\tau} \operatorname{erf} c(\sqrt{\tau}) \\ & + \frac{I_1}{\delta k} \frac{h'}{(\gamma'+h'^2)(1-h')} e^{h'^2\tau} \operatorname{erf} c(h'\sqrt{\tau}) \end{aligned} \tag{2.27}$$

where $\gamma' = \frac{\gamma}{\alpha \delta^2}$. Equation 2.27 satisfies the convection boundary condition for zero ambient temperature $(T_o = 0)$. Equations 2.25 and 2.27 can be used to compute the dimensionless surface temperature profiles at the surface for half and full laser heating pulses.

2.2.2 Laser Repetitive Pulse Heating

Laser repetitive pulse heating of the solid surface with convective boundary condition at the surface is considered to account for the assisting gas jet effect. A closed form solution for laser heating process is obtained using a Laplace transformation method in line with the previous study [1]. The conditions for constant temperature heating at the surface are investigated and the pulse parameter $\left(\frac{\beta_0}{\gamma_0}\right)$ resulting in possible steady temperature attainment at the surface is discussed.

In order to account for the repetitive pulse heating, the intensity profile resembling the consecutive pulses should be incorporated [3]. This can be achieved introducing a time shift in the intensity function, which is given in

Eq. 2.2. Therefore, the heat transfer equation employing the consecutive pulses can be written as [3]:

$$\frac{\partial^2 T}{\partial x^2} + \frac{I_1 \delta}{k}(e^{-\beta t} - e^{-\gamma t})e^{\delta x} F(t - t_o) = \frac{1}{\alpha}\frac{\partial T}{\partial t} \tag{2.28}$$

where $F(t - t_o)$ is a step function, which aids to resemble the consecutive pulses, i.e.:

$$F(t - t_o) = \left\{ \begin{array}{l} 0,\ t < t_o \\ 1,\ t \geq t_o \end{array} \right\} \tag{2.29}$$

The solution of Eq. 2.28 is identical to Eq. 2.22 provided that the time term is replaced by $(\tau - \tau_o)$ and the solution is multiplied by a non-dimensional step function. The solution of Eq. 2.28 for the surface temperature yields:

$$T(0,\tau) = F(\tau - \tau_o)\left\{ \begin{array}{l} \frac{I_1}{\delta k}\frac{1}{(1+\beta_o)(\beta_o + h_o^2)}\left[\begin{array}{c} (h_o - \beta_o)e^{-\beta_o(\tau-\tau_o)} \\ + \frac{2}{\sqrt{\pi}}\sqrt{\beta_o}(1+h_o)F(\sqrt{\beta_o(\tau-\tau_o)}) \end{array} \right] \\ \quad + \frac{I_1}{\delta k}\frac{1}{(1-h_o)(1+\beta_o)} e^{\tau-\tau_o}\mathrm{erf}\, c(\sqrt{\tau-\tau_o}) \\ \quad + \frac{I_1}{\delta k}\frac{h_o}{(\beta_o + h_o^2)(1-h_o)} e^{h_o^2(\tau-\tau_o)}\mathrm{erf}\, c(h_o\sqrt{\tau-\tau_o}) \\ + \frac{I_1}{\delta k}\frac{1}{(1+\gamma_o)(\gamma_o + h_o^2)}\left[\begin{array}{c} (h_o - \gamma_o)e^{-\gamma_o(\tau-\tau_o)} \\ + \frac{2}{\sqrt{\pi}}\sqrt{\gamma_o}(1+h_o)F(\gamma_o(\tau-\tau_o)) \end{array} \right] \\ \quad + \frac{I_1}{\delta k}\frac{1}{(1-h_o)(1+\gamma_o)} e^{\tau-\tau_o}\mathrm{erf}\, c(\sqrt{\tau-\tau_o}) \\ \quad + \frac{I_1}{\delta k}\frac{h_o}{(\gamma_o + h_o^2)(1-h_o)} e^{h_o^2(\tau-\tau_o)}\mathrm{erf}\, c(h_o\sqrt{\tau-\tau_o}) \end{array} \right\} \tag{2.30}$$

where $F(\tau - \tau_o) = \left\{ \begin{array}{l} 0,\ \tau < \tau_o \\ 1,\ \tau \geq \tau_o \end{array} \right\}$ and $\tau_o = \alpha\delta^2 t_o$.

Equation 2.30 is used to compute the dimensionless surface temperature profiles at the surface for a complete laser heating pulse.

In order to determine the peak temperature differences and the maximum temperature difference in the surface temperature profile due to repetitive pulses, the followings are introduced:

$$\Delta T_{p1} = T_{p1} - T_{p2} \tag{2.31}$$

where ΔT_{p1} is the first peak temperature difference, T_{p1} and T_{p2} are the peak surface temperatures corresponding to the first and second consecutive pulses, respectively. The second peak temperature difference can be written as:

$$\Delta T_{p2} = T_{p2} - T_{p3} \tag{2.32}$$

where T_{p3} is the peak surface temperatures corresponding to the third consecutive pulse. The maximum temperature difference in between the first and second peaks of the temperature profile is:

$$\Delta T_{\max 1} = T_{p1} - T_{\min 1} \tag{2.33}$$

where $T_{\min 1}$ is the minimum surface temperature in between the first and second consecutive pulses. The maximum temperature difference in between the second and third peaks of the temperature profile is:

$$\Delta T_{\max 2} = T_{p2} - T_{\min 2} \tag{2.34}$$

where $T_{\min 2}$ is the minimum surface temperature in between the second and third consecutive pulses.

2.3 Effect of Duty Cycle on Heating: Numerical Treatment

In practical laser heating situations, laser pulses employed have single duty cycle (energy in per pulse or energy content of a single pulse) and cycle frequency. It has been demonstrated that the repetition rate of laser pulses improves the laser processing efficiency. However, the laser pulses, in general, have a rise and a fall times, which make the analytical solution difficult to achieve, particularly for two-dimensional axisymmetric heating situations. Therefore, numerical solution for such heating situation becomes unavoidable. Since the heating process is transient, initial and boundary conditions become important resembling the actual physical process.

Consider the laser repetitive pulse heating of solid surface, the governing equation of heat diffusion consistent with the conduction limited heating situation can be written for a two-dimensional semi-infinite solid. Laser beam power intensity distribution at the solid surface can be assumed to be Gaussian with its spot center at the center of the coordinate system. The transient heat conduction equation for a solid substrate irradiated by a laser beam with a Gaussian intensity profile at the surface can be written as:

$$\rho Cp \frac{\partial T}{\partial t} = k\left[\frac{1}{r}\frac{\partial}{\partial r}\left(r\frac{\partial T}{\partial r}\right) + \frac{\partial^2 T}{\partial x^2}\right] + S_0 \tag{2.35}$$

where x is the axial direction (along the laser beam axis), r is the radial direction (normal to the laser beam axis) ρ is the density, k is the thermal conductivity, Cp is the specific heat and S_0 is the volumetric source term. The volumetric heat source can be arranged to resemble the laser repetitive pulses; therefore,

$$S_0 = I_0 f(t)\delta\left(1 - r_f\right)\exp(-\delta x)\exp\left(-\frac{r^2}{a^2}\right) \tag{2.36}$$

where I_0, δ, r_f and a are the power intensity, absorption depth and the Gaussian parameter, respectively.

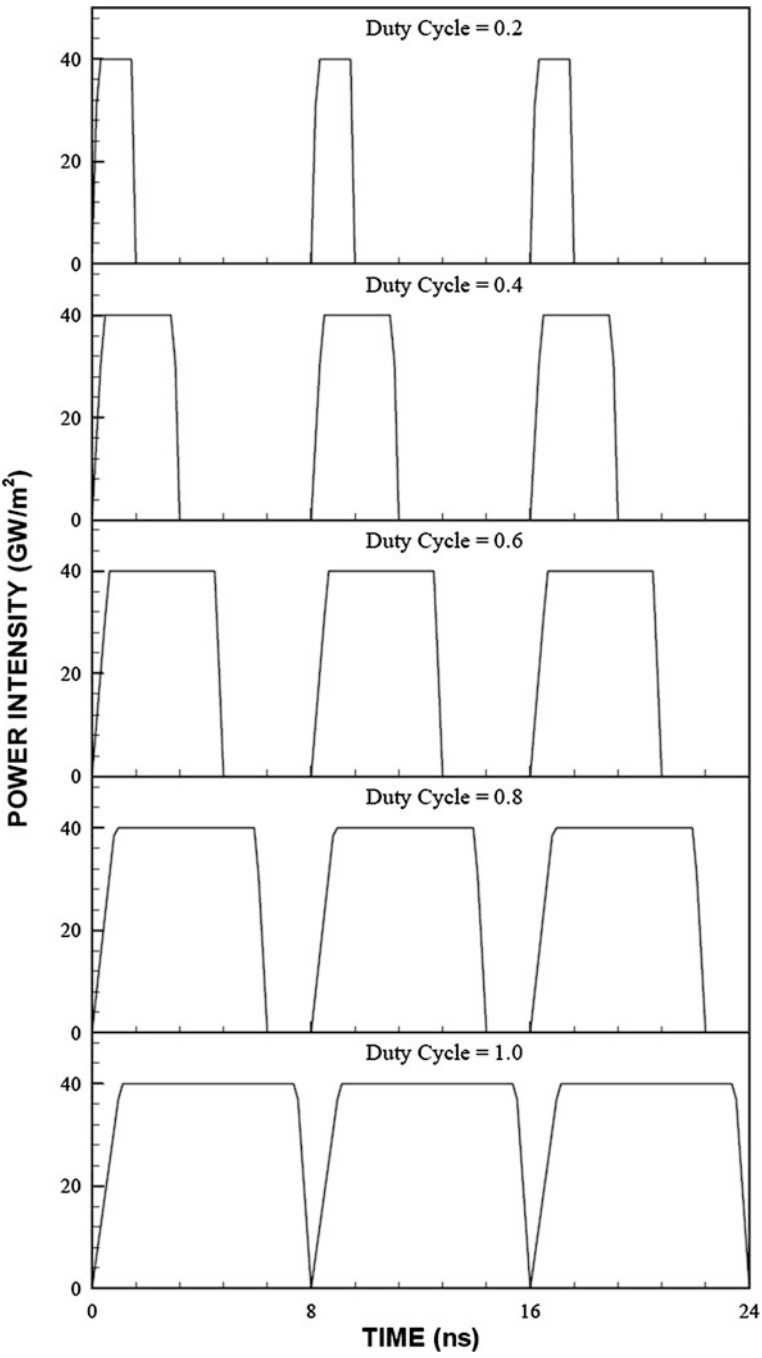

Fig. 2.1 Laser pulses with five duty cycles for the first three consecutive pulses

The temporal variation of pulse intensity resembling laser repetitive pulses can be defined by the function $f(t)$, which is:

$$f(t) = \left\{ \begin{array}{ll} 0 \leq t \leq t_r & at \\ -t_r < t \leq t_p & 1 \\ t_p < t \leq t_f & -bt \\ t_f < t < t_c & 0 \end{array} \right\} \tag{2.37}$$

where t_r and t_f are the constants defining the rise and fall of the laser pulse, t_p is the pulse length, and a and b are the constants. The pulse shape used in the simulation is shown in Fig. 2.1.

The initial condition can be represented as the substrate material is assumed to be initially ($t = 0$) at a uniform temperature T_0 which can be specified.

In order to represent the assisting gas, a convective boundary condition is assumed at the surface ($x = 0$). The heat transfer coefficient used in the present simulations is $h = 10^4$ W/m^2K [1]. Therefore, at the surface, where $x = 0$, the boundary condition yields $\frac{\partial T}{\partial x} = h(T_s - T_0)$.

At the symmetry axis ($r = 0$) temperature is assumed to be maximum. Therefore, at the symmetry axis ($r = 0$), the boundary condition is $\frac{\partial T}{\partial r} = 0$. At a distance far away from the surface distance significantly larger than the absorption depth of the substrate material (δ), a room temperature is assumed, i.e. as $x \rightarrow \infty$ $T = T_0$.

Equation 2.35 is simulated numerically to obtain thermal response of the substrate material due to the repetitive heating pulse.

The numerical scheme employing an implicit formulation is used. To discretize the governing equations, a control volume approach is introduced. The calculation domain is divided into grids and grid independence test is being performed for different grid size and orientation. A non-uniform grid with 95 × 80 mesh points along x and r axes, respectively, is employed after securing the grid independence. The finer grids are located near the irradiated spot center in the vicinity of the surface and grids become courser as the distance increases towards the bulk of substrate material. A computer program based on implicit scheme is used to compute the temperature field.

2.4 Discussions

The comparison of the analytical solutions with the literature [4, 5] and temperature predictions from the analytical solutions are presented in line with the previous studies [1, 2, 6]. The findings in relation to analytical solutions and the numerical predictions are discussed according to the sub-headings given below.

2.4.1 Exponential Pulse Heating Case and Convection Condition Resembling Assisting Gas at the Surface

The closed-form solution for the temperature profiles due to time exponentially varying pulse is obtained. In order to account for the pulse resembling a typical actual pulse, two different time exponentially varying pulse intensities are considered. The heating involved with the time exponentially varying pulse, having a single time exponential term, is called the half pulse case while for the time exponentially varying pulse, having two time exponential terms, is called the full pulse case in the discussion section. The closed-form solution obtained is compared with the analytical solutions reported in the literature for different heating conditions [4, 6]. The data used in the solutions are given in Table 2.1.

To deduce the closed-form solution derived from the present analysis to the analytical solutions reported in the literature, the following heating conditions are considered: (1) step input intensity pulse with convective boundary condition at the surface, and (2) time exponentially varying pulse with non-convective boundary condition at the surface. The analytical solution for the step input intensity pulse with convective boundary condition was obtained previously by Blackwell [4]. In order to introduce the step input intensity pulse in the closed-form solution derived at present, the pulse parameters (β' and γ') in the source term of Eq. 2.2 or in the closed-form solution Eq. 2.25 should be set to zero. Moreover, the initial and ambient temperatures, and the symbol of absorption coefficient used in Blackwell's solution are different than those employed in the present analysis, i.e. the initial temperature is set to zero, the ambient temperature is denoted as T_0 and δ is used for the absorption coefficient in the present study. The resulting equation is:

$$
\begin{aligned}
T(x,t) = & T_o\left[\operatorname{erfc}\left(\frac{x}{2\sqrt{\alpha t}}\right) - e^{\left(\frac{h^2}{k^2}\alpha t + \frac{h}{k}x\right)}\operatorname{erfc}\left(\frac{x}{2\sqrt{\alpha t}} + \frac{h}{k}\sqrt{\alpha t}\right)\right] \\
& + \frac{I_1}{k\delta}\left\{\begin{array}{c}
\left(1+\frac{k\delta}{h}\right)\operatorname{erfc}\left(\frac{x}{2\sqrt{\alpha t}}\right) - \frac{1}{2}e^{(\alpha\delta^2 t - \delta x)}\operatorname{erfc}\left(-\delta\sqrt{\alpha t} + \frac{x}{2\sqrt{\alpha t}}\right) \\
-\frac{1}{2}\frac{\left(\frac{h}{k\delta}+1\right)}{\left(\frac{h}{k\delta}-1\right)}e^{(\alpha\delta^2 t + \delta x)}\operatorname{erfc}\left(\delta\sqrt{\alpha t} + \frac{x}{2\sqrt{\alpha t}}\right) \\
+\frac{1}{\frac{h}{k\delta}\left(\frac{h}{k\delta}-1\right)}e^{\left(\frac{h}{k}x + \frac{h^2}{k^2}\alpha t\right)}\operatorname{erfc}\left(\frac{h}{k}\sqrt{\alpha t} + \frac{x}{2\sqrt{\alpha t}}\right) + e^{-\delta x}\left(e^{\alpha\delta^2 t} - 1\right)
\end{array}\right\}
\end{aligned}
\tag{2.38}
$$

Equation 2.38 is identical to the analytical solution obtained by Blackwell [4].

Table 2.1 Data used in the solutions for exponential pulse heating

Substrate	$\delta \times 10^7$ (1/m)	$\alpha \times 10^{-4}$ (m^2/s)	c_p (J/kgK)	ρ (kg/m^3)	k (1/s)	γ (1/s)	I_0 (W/m^2)	
Steel	6.16	0.227	460	7,880	80.3	0.1–0.3	0.3	10^{11}

The analytical solution for the non-convective boundary condition at the surface and time exponentially varying intensity pulse was obtained by Yilbas [6] previously. To introduce the non-convective boundary condition at the surface, the heat transfer coefficient (h) in Eq. 2.25 is set to zero. In this case, for a half pulse, Eq. 2.25 reduces to:

$$T(0,\tau) = \frac{I_1}{k\delta(1+\beta')}\left[e^{\tau}\mathrm{erfc}(\sqrt{\tau}) + \frac{2}{\sqrt{\pi}}\frac{1}{\sqrt{\beta'}}F\left(\sqrt{\beta'\tau}\right) - e^{-\beta'\tau}\right] \tag{2.39}$$

Equation 2.39 is identical to the analytical solution obtained previously by Yilbas [6].

Figure 2.2 shows the temporal variation of the surface temperature for the half pulse case and constant heat transfer coefficient $\left(h = 10^4\ \mathrm{W/m^2K}\right)$ at the surface while pulse parameter (β') is variable. In general, the rise of the temperature profiles is similar during the initial period of heating. As β' reduces, temperature reaches its peak value earlier. This occurs because of the time variation of the heating pulse as depicted in Fig. 2.3. In this case, as β' increases, the power intensity distribution leans towards the pulse beginning provided that the area under the pulse intensity curve becomes less. Consequently, the energy content of the heating pulse reduces as β' increases, which in turn results in low peak temperature at the surface of the substrate. The rate of surface temperature rise and decay varies as β' varies. This can also be seen from Fig. 2.4, in which $\frac{\partial T}{\partial \tau}$ with time (τ) is shown. $\frac{\partial T}{\partial \tau}$ decays rapidly as τ increases from the pulse beginning. The slope of $\frac{\partial T}{\partial \tau}$ curve reduces to zero at time corresponding to the peak temperature. The duration at which rapid decay of $\frac{\partial T}{\partial \tau}$ indicates the rapid increase of internal energy gain of the substrate, which dominates over the conduction and convection energy transport. At the time of minimum $\frac{\partial T}{\partial \tau}$, internal energy gain of the substrate becomes considerably small, since the pulse energy corresponding to this heating

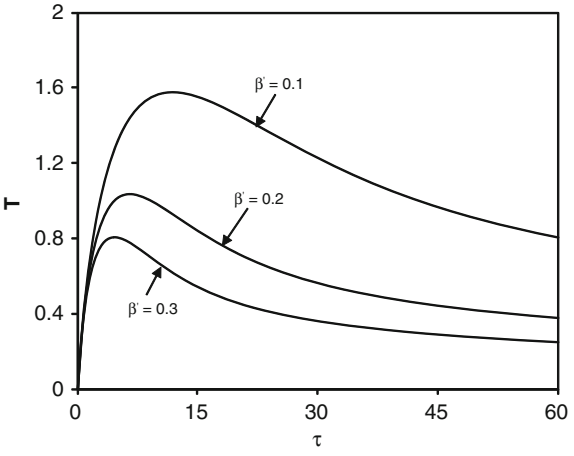

Fig. 2.2 Temporal variation of temperature for $\mathrm{Bi} = 2 \times 10^{-5}$ and β' is variable

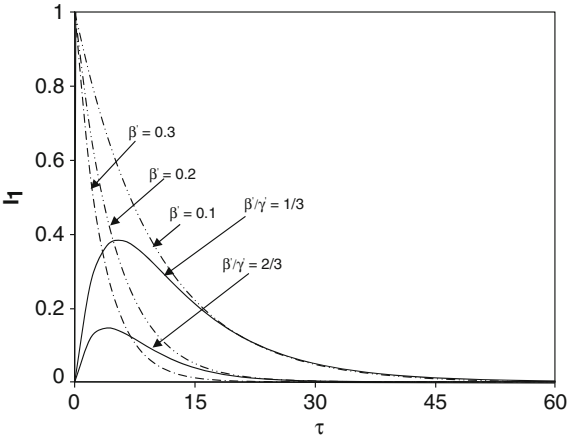

Fig. 2.3 Temporal variation of power intensity distribution as β', γ' and β'/γ' are variable

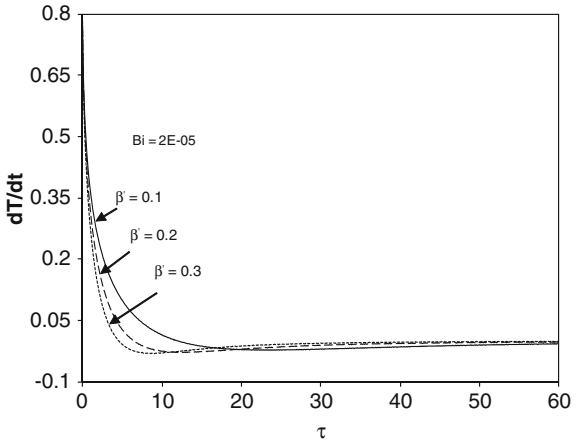

Fig. 2.4 Temporal variation of time gradient of temperature for $Bi = 2 \times 10^{-5}$and different β' values

time is very small. As pulse intensity ceases, the conduction and convection become the sole mechanisms in energy transport process. In accordance with the previous study [7], the equilibrium time can be introduced at the point of minimum $\frac{\partial T}{\partial \tau}$. In this case, the energy balance attains among the internal energy gain, due to absorption of laser pulse, conduction, and convection contribution of the energy transport in the surface vicinity of the substrate. The equilibrium time shifts close to the pulse beginning as β' reduces. This is due to the temporal distribution of the laser pulse intensity as indicated earlier.

Figure 2.5 shows the temporal variation of surface temperature for different values of Biot number (B_i) and fixed β' value. The effect of Bi on the temperature profiles is not significant for $Bi \leq 0.02$. This because the energy absorbed by the substrate, which is considerably high as compared to the energy transported due to convection from the surface of the substrate. However, as Bi increases further, the

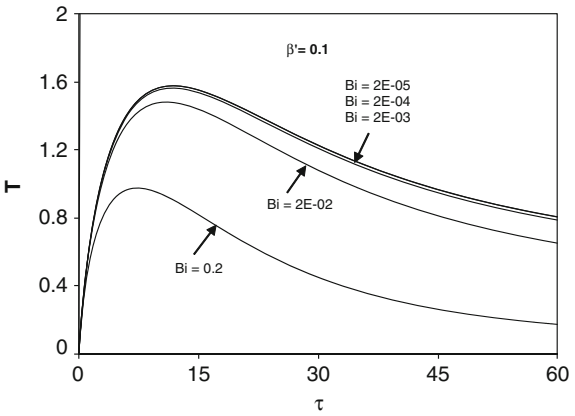

Fig. 2.5 Temporal variation of temperature for different $\beta' = 0.1$ and Biot number

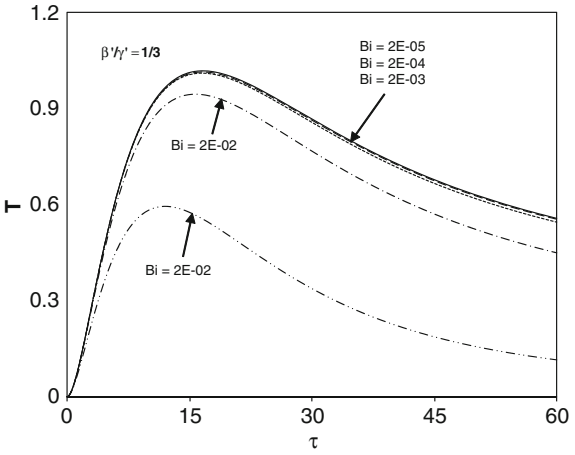

Fig. 2.6 Temporal variation of temperature for $\beta'/\gamma' = 1/3$ and Biot number is variable

rate of rise and the value of peak temperature at the surface reduce. In this case, energy transported from the surface because of convection becomes considerable. The time corresponding to peak temperature moves close to the pulse beginning for high Bi.

In order to resemble the actual laser pulse, a full pulse is considered; in which case, the pulse profile $I = I_1[\exp(-\beta'\tau) - \exp(-\gamma'\tau)]$ is employed in the source term of Eq. 2.1. Figure 2.6 shows the temporal variation of temperature profiles at the surface obtained for full pulse profile, in which $\beta' = 0.1$ and $\gamma' = 0.3$ are employed. The rate of change of temperature profile in the pulse beginning is lower than that corresponding to a half pulse for $\beta' = 0.1$. This is because the power intensity corresponding to a half pulse is higher than its counterpart corresponding to a full pulse Fig. 2.3. As similar to the behavior of Bi for the half pulse, the effect of Bi on temperature profiles is more pronounced as $Bi \geq 0.03$. The equilibrium time, as defined earlier, for a full pulse varies with changing B_i.

The equilibrium time corresponding to low β', $\frac{\beta'}{\gamma'}$ and high Bi is small. This indicates that early rise of the pulse intensity results in small equilibrium time. Moreover, high value of Bi reduces the equilibrium time for half and full pulses. In this case, convection cooling of the surface suppresses the internal energy gain of the substrate. Consequently, the domination of the internal energy gain in the energy transport process ceases earlier during the heating pulse.

2.4.2 Repetitive Pulse Heating Case and Convection Condition Resembling Assisting Gas at the Surface

In order to obtain a constant temperature heating condition at the surface, the laser repetitive pulses with constructively decaying peak intensities are considered. To account for the cooling of the surface, the Biot number (Bi) is varied in between 0.2 and 2×10^{-4}, the pulse parameters $\left(\frac{\beta_0}{\gamma_0}\right)$ is varied in between 2.5 and 6, and the ratios of peak pulse intensity of consecutive pulses are $\frac{I_{02}}{I_{01}} = 0.25$ and $\frac{I_{03}}{I_{01}} = 0.0625$, respectively. Table 2.2 gives the data used in the solutions of temperature field. The second pulse of the consecutive pulses starts once the first pulse ends or about to end. The overlapping of the consecutive pulses is minimal. This is, however, more pronounced when $\frac{\beta_0}{\gamma_0}$ reduces as seen from Fig. 2.7, in which the power intensity distribution with time is shown. It should be noted that the energy content of the overlapping portion of the repetitive pulses is only a fraction of the respective repetitive pulses, which overlap.

Figure 2.8 shows the temporal variation of the non-dimensional surface temperature $\left(\frac{T}{I_0/k\delta}\right)$ for three consecutive pulses with $\frac{\beta_0}{\gamma_0} = 4$, and Bi as variable while Fig. 2.9 shows the time derivative of temporal variation of the non-dimensional surface temperature for the same condition of Fig. 2.8. The peak temperature increases as Bi reduces. This is because the rate of convective cooling of the surface, which reduces as Bi reduces, i.e. the heat transfer coefficient reduces. The effect of Bi on temperature profile is less pronounced as Bi reduces to 10^{-3} and beyond. In this case, the convective cooling of the surface does not substantiate and the internal energy gain dominates over the convective cooling of the surface. As Bi increases, the convective cooling of the surface becomes as important as the internal energy gain of the substrate material, which in turn reduces the peak temperature at the surface. When comparing the trend of the temperature profiles

Table 2.2 Data used in the solutions of the repetitive pulse heating

Bi	$\delta \times 10^7$ (1/m)	$\alpha \times 10^{-4}$ (m^2/s)	c_p (J/kgK)	ρ (kg/m^3)	k (W/mK)	β_0 (1/s)	γ_0 (1/s)	I_o (W/m^2)	τ_0
0.2–2 $\times 10^{-4}$	6.16	0.227	460	7,880	80.3	0.3	0.05–0.125	4.5×10^{12}	40

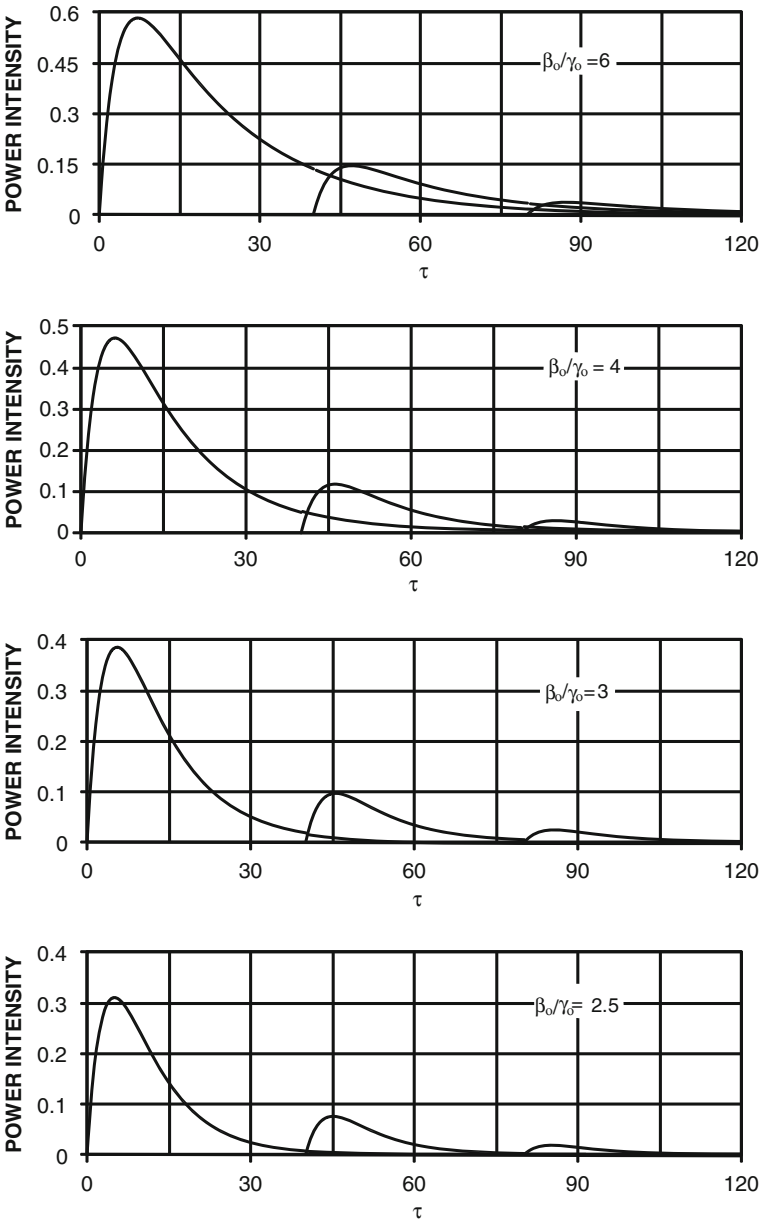

Fig. 2.7 Temporal variation of dimensionless intensity as β_0/γ_0 variable

with time due to consecutive pulses and different *Bi*, the surface temperature shows an increasing trend with time as *Bi* reduces. The trend becomes almost steady with some fluctuations across the peak temperatures for $Bi = 2\times10^{-2}$. The

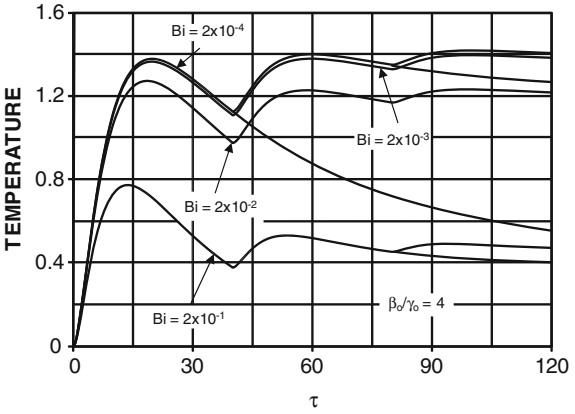

Fig. 2.8 Temporal variation of dimensionless surface temperature for $\beta_0/\gamma_0 = 4$ and *Bi* variable

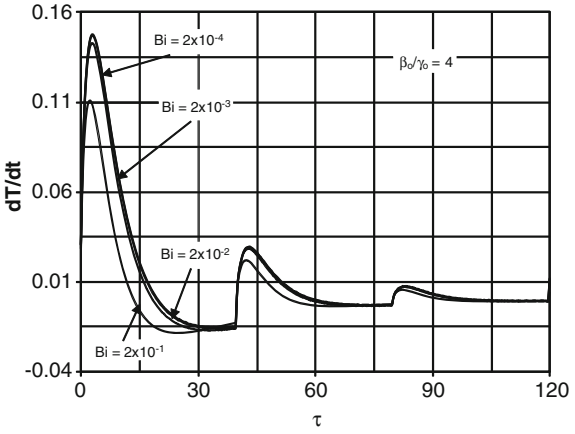

Fig. 2.9 Temporal variation of time derivative of dimensionless surface temperature for $\beta_0/\gamma_0 = 4$ and *Bi* variable

further reduction in *Bi* results in decreasing trend with time in surface temperature profile. Consequently, the convective cooling does not lower the peak value of the surface temperature only, but effects the temporal behavior of the surface temperature resulted from the consecutive pulses. In the case of $\frac{\beta_0}{\gamma_0} = 6$ Fig. 2.10, the surface temperature due to consecutive pulses shows increasing trends with time for $Bi \leq 10^{-2}$, and the trend becomes almost steady with time for $Bi = 0.2$. Consequently, increasing $\frac{\beta_0}{\gamma_0}$ results in increasing peak temperature and the surface temperature profile due consecutive pulses shows an increasing trend with time. In the case of high *Bi* $(Bi = 0.2)$, the surface temperature attain almost steady trend with time.

Figures 2.11, 2.12, and 2.13 show the first peak temperature difference $\left(\Delta T_{p1}\right)$, second peak temperature difference $\left(\Delta T_{p2}\right)$, the maximum temperature difference in between the first and second peak temperatures $(\Delta T_{\max 1})$, and the maximum temperature difference in between second and third peak temperatures $(\Delta T_{\max 2})$

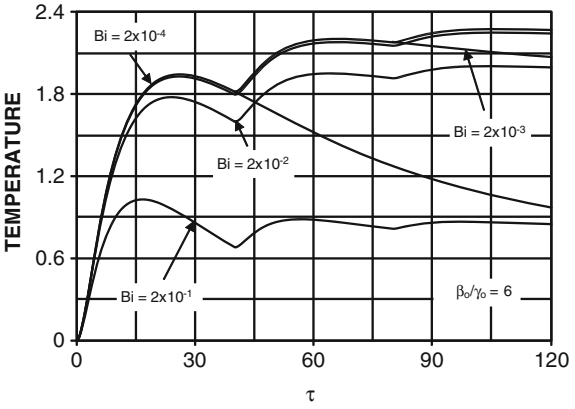

Fig. 2.10 Temporal variation of dimensionless surface temperature for $\beta_0/\gamma_0 = 6$ and *Bi* variable

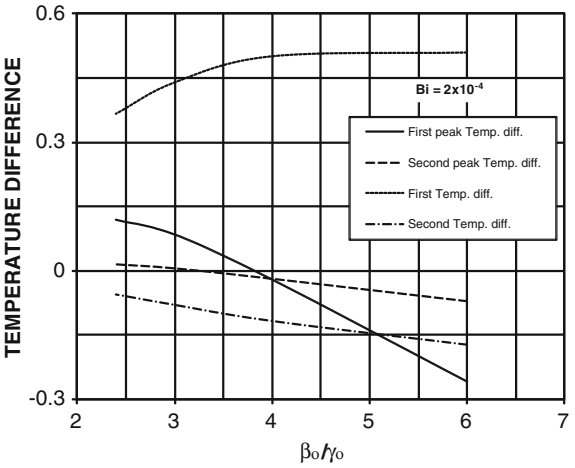

Fig. 2.11 Dimensionless surface temperature difference with β_0/γ_0 and $Bi = 2 \times 10^{-4}$

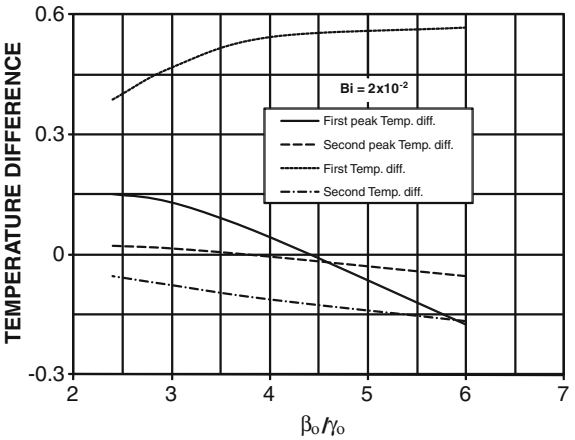

Fig. 2.12 Dimensionless surface temperature difference with β_0/γ_0 and $Bi = 2 \times 10^{-2}$

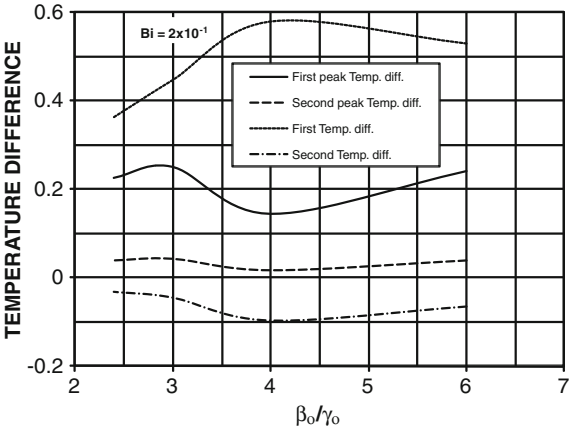

Fig. 2.13 Dimensionless surface temperature difference with β_0/γ_0 and $Bi = 2 \times 10^{-1}$

with $\frac{\beta}{\gamma}$ as Bi variable. ΔT_{p1} is positive for $\frac{\beta_0}{\gamma_0} \leq 4$ and this reverses for $\frac{\beta_0}{\gamma_0} > 4$. This is also true for ΔT_{p2} as $Bi \geq 10^{-3}$. This indicates that the first peak temperature is always greater than the second peak temperature for $\frac{\beta_0}{\gamma_0} < 4$, i.e. the temperature profile shows an increasing trend with time. However, ΔT_{p1} becomes zero for $\frac{\beta_0}{\gamma_0} = 4.5$ for $Bi = 2 \times 10^{-2}$ and $Bi \leq 2 \times 10^{-3}$. In the case of ΔT_{p2}, it becomes zero at $\frac{\beta_0}{\gamma_0} = 3.25$ for $Bi \leq 2 \times 10^{-3}$. Therefore, as Bi increases $\frac{\beta_0}{\gamma_0}$ also increases for the zero value of ΔT_{p1} and ΔT_{p2}. In the case of $Bi = 0.2$, first peak temperature difference is always positive for $\frac{\beta_0}{\gamma_0}$ and this is also true for ΔT_{p2}. Consequently, the surface temperature has a decreasing trend with time. $\Delta T_{\max 1}$ attains large values as Bi reduces. Moreover, $\Delta T_{\max 1}$ increases with increasing $\frac{\beta_0}{\gamma_0}$. As $\frac{\beta_0}{\gamma_0}$ increases, the time corresponding to the peak temperature moves towards the pulse beginning as seen from Fig. 2.8. Consequently, high peak intensity differences results in large peak temperature and maximum temperature differences in the surface temperature profiles. ΔT_{p2} is relatively smaller than ΔT_{p1}. In general, a steady temperature at the surface is unlikely to occur, since $\Delta T_{\max 1}$ and ΔT_{p1} attain high values, which in turn results in large fluctuation in the temperature profile. However, the magnitude of fluctuation becomes less as $\frac{\beta_0}{\gamma_0}$ and Bi reduce.

2.4.3 *Effect of Duty Cycle on Heating and Convection Condition Resembling Assisting Gas at the Surface*

Table 2.3 gives the data used in the numerical simulations. Figure 2.14 shows temporal variation of surface temperature for different duty cycles of laser pulses. The rise of surface temperature is high in the early heating period for all duty

Table 2.3 Data used for the numerical predictions for the effect of the duty cycle on temperature

$\delta \times 10^7$ (1/m)	c_p (J/kgK)	ρ (kg/m^3)	k (W/mK)	β (1/s)	h (W/m^{2}K)	a (1/m)	γ (1/s)	I_o (W/m^2)
6.16	330	7,836	52	0.1	10^4	0.0707	0.05	4×10^{10}

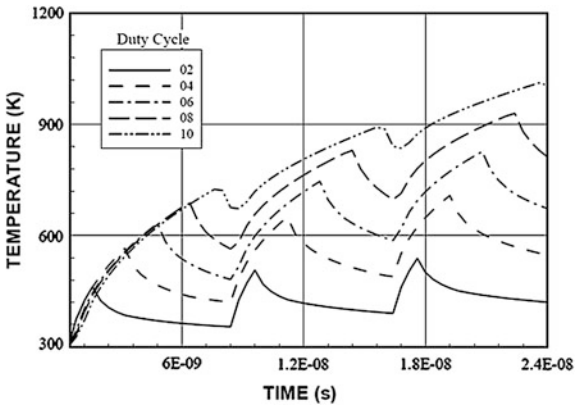

Fig. 2.14 Temporal variation of surface temperature at symmetry axis for the first three pulses

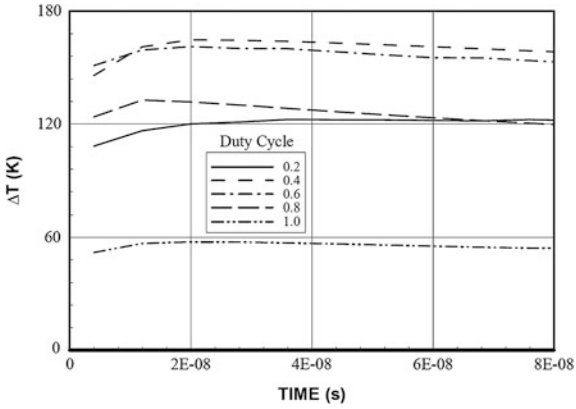

Fig. 2.15 Temporal variation of surface temperature difference (ΔT) at the symmetry axis for the first ten pulses and different duty cycles

cycles and as the pulse progresses towards its ending, the rate of rise becomes steady. The high rate of temperature rise is associated with the internal energy gain and temperature gradient in the surface region of the substrate material. In this case, energy absorbed by the substrate material is high in the surface region due to Lambert's Law, which in turn, increases the internal energy gain substantially in this region. In the early heating period, temperature gradient is low, and diffusional energy transfer, due to temperature gradient, from the surface region to solid bulk becomes less. This enhances the temperature rise. However, as the heating progresses, temperature gradient increases accelerating the diffusional energy transfer from surface region to the solid bulk. Although, increasing duty cycle increases the laser energy in the pulse, enhancing the magnitude of temperature, the rate of

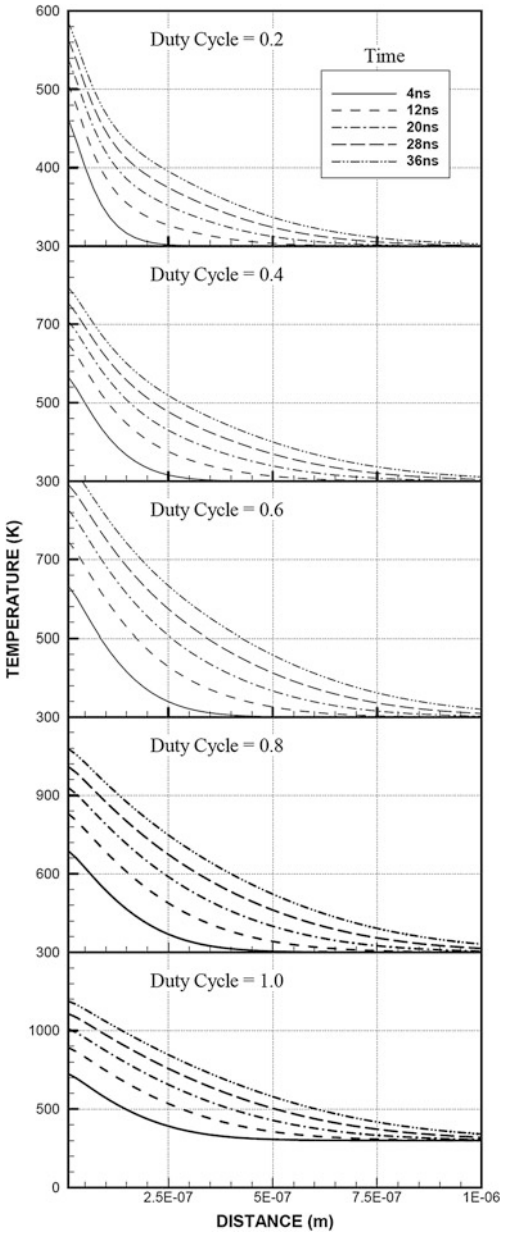

Fig. 2.16 Temperature variation along the symmetry axis inside the substrate material for different heating periods and duty cycles

temperature rise in both early and late heating periods changes. This indicates that increasing duty cycle enhances temperature rise in a short duration at the substrate surface.

Figure 2.15 shows temporal variation of temperature difference at the surface for different duty cycles. Temperature difference is calculated as the difference

between the maximum temperature in a pulse and the temperature at the corresponding pulse ending. Temperature difference remains almost constant with time despite the fact that maximum temperature at the surface increases. This indicates that the thermal response of the surface to the heating pulse becomes the same with a given duty cycle of the consecutive pulses. Moreover, as the duty cycle increases, the magnitude of temperature also increases. Once the duty cycle is kept constant for the pulses, the temperature difference remains almost constant with time. The high magnitude of temperature difference results in cyclic thermal loading of the surface. Consequently, thermal integration (steady rise of surface temperature during repetitive pulses) at the surface replaces with thermal loading of the surface. This situation results in thermal fatigue of the surface. Therefore, increasing duty cycle enables surface temperature to rise at high rates; but, it causes cyclic thermal loading at the surface due to magnified temperature difference.

Figure 2.16 shows temperature distribution inside the substrate material for different duty cycles and heating periods when temperature is maximum at the surface. Temperature profiles are plotted when surface temperature is maximum for a given time period. The temperature gradient attains large values, particularly in the surface region for small duty cycles. The temperature gradient attains minimum at some depths below the surface and as the heating duration progresses, the location of minimum temperature gradient moves away from the surface. The energy balance is attained at the point of minimum temperature gradient such that internal energy gain from the irradiated field balances the diffusional energy loss from the surface region to the solid bulk. Consequently, the diffusional energy transfer dominates the energy transfer process in the region beyond the location of minimum temperature gradient. Moreover, increasing duty cycle does not alter the location of minimum temperature gradient considerably in the substrate material. This indicates that the duty cycle change the magnitude of temperature gradient; however, the location of maximum temperature gradient remains almost the same in the substrate material for different duty cycles. Consequently, amount of energy transport in the surface region enhances with increasing duty cycle, but energy transport by diffusion becomes important at the particularly location inside the substrate material for all duty cycles.

References

1. Kalyon, M., Yilbas, B.S.: Analytical solution for laser evaporative heating process: time exponentially decaying pulse case. J. Phys. Part D: Applied Physics **34**, 3303–3311 (2001)
2. Kalyon, M., Yilbas, B.S.: Repetitive laser pulse heating analysis: pulse parameter variation effects on closed form solution. Appl. Surf. Sci. **252**, 2242–2250 (2006)
3. Yilbas, B.S., Shuja, S.Z.: Laser short-pulse heating of surfaces. J. Phys. D Appl. Phys. **32**, 1947–1954 (1999)
4. Blackwell, F.J.: Temperature profile in semi-infinite body with exponential source and convective boundary conditions', ASME. J. Heat Transfer **112**, 567–571 (1990)

5. Shuja, S.Z., Yilbas, B.S., Shazli, S.Z.: Laser repetitive pulse heating influence of pulse duty. Heat Mass Transf. **43**, 949–955 (2007)
6. Yilbas, B.S.: Analytical solution for time unsteady laser pulse heating of semi-infinite solid. Int. J. Mechanical Sciences **39**(6), 671–682 (1997)
7. Yilbas, B.S., Sami, M.: 3-Dimensional laser heating including evaporation—a kinetic theory approach. Int. J. Heat and Mass Transf. **41/13**, 1969–1981 (1998)

http://www.springer.com/978-3-642-36628-4

Laser Surface Processing and Model Studies

Yilbas, B.S.; Shuja, S.Z.
2013, IX, 147 p., Hardcover
ISBN: 978-3-642-36628-4